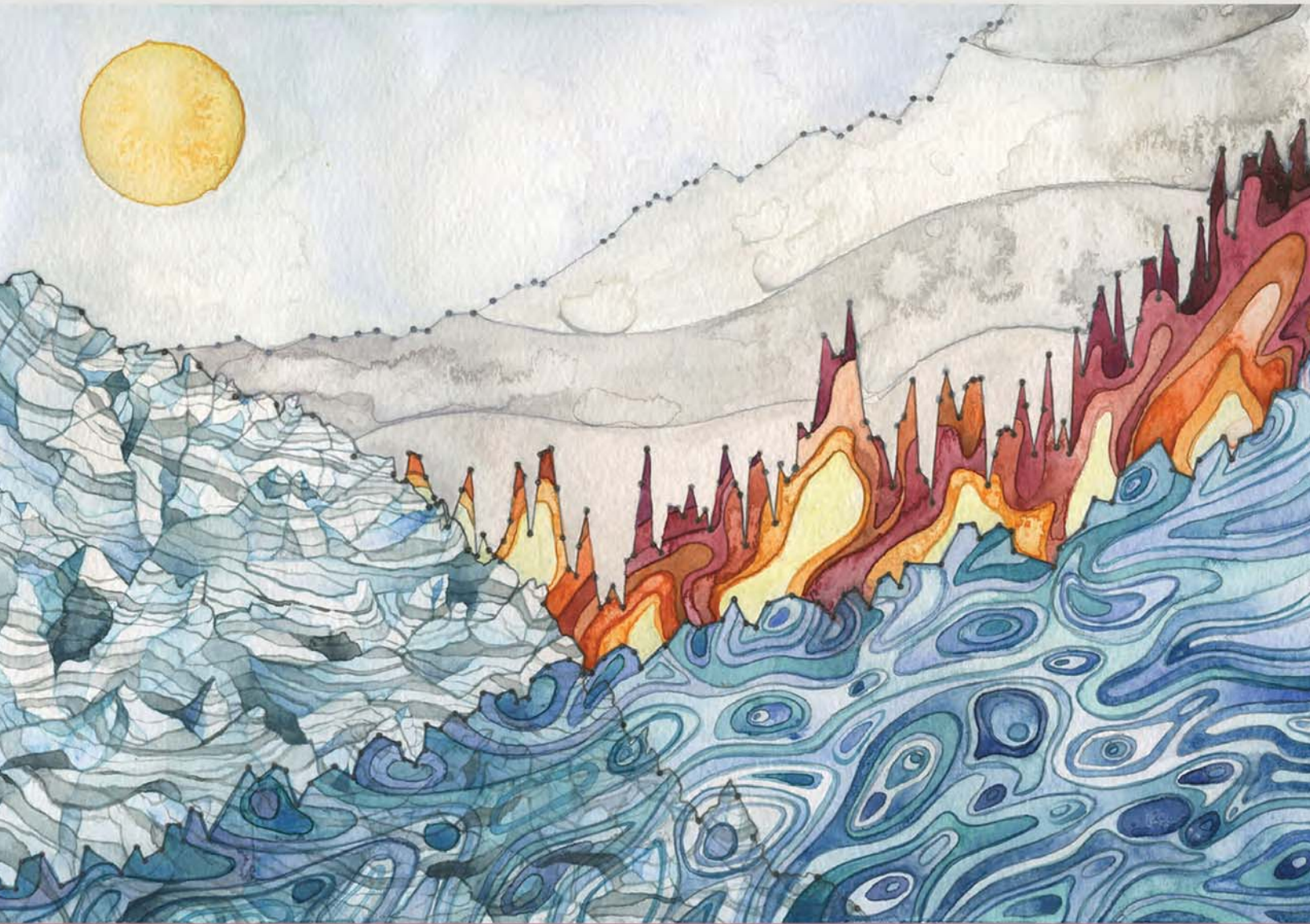


STATE OF THE CLIMATE IN 2015



Special Supplement to the
Bulletin of the American Meteorological Society
Vol. 97, No. 8, August 2016

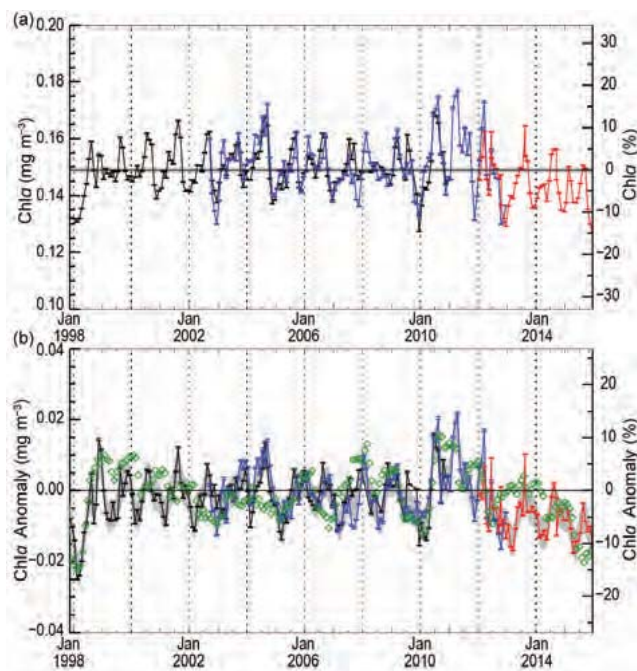


FIG. 3.27. Eighteen-year, multimission record of Chla averaged over the PSO (see Fig. 3.25) for (black) SeaWiFS, (blue) MODISA, and (red) VIIRS. (a) Independent records from each mission, with the multimission mean Chla concentration for the region (horizontal black line). (b) Monthly anomalies for SeaWiFS, MODISA, and VIIRS after subtraction of the 9-year MODISA monthly climatological mean (2003–11), with the averaged difference between SeaWiFS and MODISA over the common mission lifetime (gray region). The MEI (green diamonds, see text) inverted and scaled to match the range of the Chla anomalies.

2015). This difference is not due to a change in global phytoplankton abundances but rather is a consequence of the R2014.0 reprocessing that includes calibration updates and a revised chlorophyll algorithm (Hu et al. 2012). The time series demonstrates the high level of consistency between the overlapping periods of the SeaWiFS and MODISA missions. Beyond 2012, the MODISA time series becomes increasingly erratic (not shown), reflecting a growing uncertainty in the calibration of that instrument (Franz et al. 2015). Consistency between MODISA and VIIRS in 2012, however, provides confidence for extension of the multimission trends into 2015.

Chla monthly anomalies within the PSO (Fig. 3.27b) exhibit variations of ~15% over the multimission time series, with climatic events such as El Niño and La Niña clearly delineated. In 2015, consistent with a strong El Niño, Chla trends in the PSO approached the lowest levels measured since the 1997/98 El Niño. Furthermore, mean Chla concentrations in the PSO declined by approximately 20% from the peak observed during the 2010/11 La Niña, con-

sistent with expectations based on multivariate ENSO index variations (MEI; Wolter and Timlin 1998).

Distinguishing the different drivers of Chla variability is important for interpreting the satellite record. Light-driven decreases in chlorophyll are associated with constant or even increased rates of photosynthesis, while nutrient-driven decreases are associated with decreased photosynthesis. An analysis of photoacclimation and nutrient-driven changes in growth rate and biomass from the MODIS record shows that the inverse relationship between SST and Chla anomalies is overwhelmingly due to light- and division rate-driven changes in cellular pigmentation, rather than changes in biomass (Behrenfeld et al. 2016). This study also shows that photoacclimation contributed 10%–80% of the variability in cellular pigmentation, suggesting the 2015 anomaly patterns in Chla for the PSO (Fig. 3.26c) were largely driven by photoacclimation. An additional contributor to the anomaly patterns in Chla is the misrepresentation of Chla changes due to colored dissolved organic matter (cDOM) signals (Siegel et al. 2005). Sunlight degrades cDOM, and this degradation is more extensive for shallow MLDs, yielding in the PSO an inverse relationship between cDOM and SST (Nelson and Siegel 2013) that may be mistakenly attributed to Chla changes (Siegel et al. 2013).

j. Global ocean carbon cycle—R. A. Feely, R. Wanninkhof, B. R. Carter, J. N. Cross, J. T. Mathis, C. L. Sabine, C. E. Cosca, and J. A. Tirranes

The global ocean is a major sink for anthropogenic carbon dioxide (CO₂) that is released into the atmosphere from fossil fuel combustion, cement production, and land-use changes. Over the last decade, the global ocean has continued to take up a substantial fraction of anthropogenic carbon (C_{anth}) emissions and is therefore a major mediator of global climate change. Air–sea flux studies, general ocean circulation models including biogeochemistry, and data-constrained inverse models suggest the ocean absorbed approximately 46 Pg C (1 Pg C ≡ 10¹⁵ grams of carbon) of C_{anth} between 1994 and 2014 (Le Quéré et al. 2015; DeVries 2014), with an increase in the rate of C_{anth} uptake from 2.2 ± 0.5 Pg C yr⁻¹ during the 1990s to approximately 2.6 ± 0.5 Pg C yr⁻¹ during the most recent decade from 2005 to 2014 (Table 3.1). A summary of the air–sea exchange and ocean inventory of C_{anth} based on both observations and model results through 2014 is presented. Data for 2015 are not available owing to the need for careful scientific quality control of ocean carbon data prior to analysis.

1) AIR-SEA CARBON DIOXIDE FLUXES

Ocean CO₂ uptake can be estimated from air-sea differences in CO₂ partial pressure ($p\text{CO}_2$) and gas transfer velocity, which is mainly a function of wind speed. Significant improvement in global and regional CO₂ flux estimates have been made in the past year as part of Surface Ocean $p\text{CO}_2$ Mapping Intercomparison (SOCOM), comparing 13 independent data-based methods of global interpolation of $p\text{CO}_2$ (Rödenbeck et al. 2015). Recent research has also decreased uncertainty on the equations used to estimate CO₂ exchange from air-sea $p\text{CO}_2$ differences (Wanninkhof 2014; Ho and Wanninkhof 2016). Large increases in autonomous $p\text{CO}_2$ measurements over time have been achieved with ships of opportunity (SOOP-CO₂) and moorings. The third update of the Surface Ocean CO₂ Atlas (SOCAT) with over 14 million data points was released to the public in 2015 (Bakker et al. 2016). Subsequent data releases will occur annually such that the data can inform the annual assessment of global CO₂ sources and sinks provided by the Global Carbon Project (www.globalcarbonproject.org). The increased data coverage and new mapping techniques make it possible to obtain air-sea CO₂ fluxes at monthly time scales, allowing investigation of variability on subannual to decadal time scales and the causes thereof. An important recent result illuminated by these improved approaches is the reinvigoration of the Southern Ocean carbon sink since 2002 (Landschützer et al. 2015), which had previously been found to be decreasing (Le Quéré et al. 2007).

The newly released datasets have been used to verify the magnitude of the anthropogenic air-sea CO₂ fluxes over the last decade and in 2014. The ocean sink in 2014 was 10% above the 2005–14 average of $2.6 \pm 0.5 \text{ Pg C yr}^{-1}$ (Table 3.1). In 2014, the ocean and land carbon sinks removed 27% and 37% of total CO₂ emissions, respectively, leaving 36% of emissions in the atmosphere, compared to 44% as a decadal average (Le Quéré et al. 2015).

Ocean uptake anomalies (Fig. 3.28b) in 2014 relative to the 2005–14 average (Fig. 3.28a) are attributed to several climate reorganizations. The lower CO₂ effluxes in the equatorial Pacific are attributed to anomalously high regional SST and reduced upwelling of CO₂-rich subsurface waters due to a weak Modoki-like near-El Niño in 2014. Stronger effluxes are evident in the northeast Pacific due to the warm “Blob” (Bond et al. 2015) as well as warm conditions offshore of the California coast (Fig. 3.29). A cold anomaly in the southern Labrador Sea and adjacent regions (Josey et al. 2015) associated with deep mix-

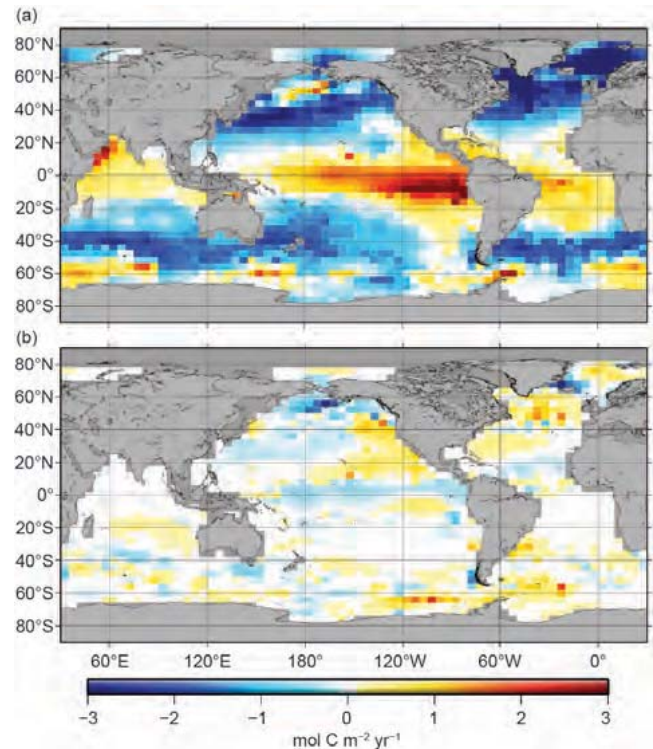


FIG. 3.28. (a) Average annual air-sea CO₂ flux for 2005–14 based on the AOML-EMP approach (Park et al. 2010). Positive values are effluxes and negative values are influxes. The SST anomaly interpolation method used for this analysis is less robust than more recent and sophisticated approaches (Rödenbeck et al. 2015), but faithfully reproduces the major anomaly features, especially in the highly data-constrained equatorial Pacific. (b) Air-sea CO₂ flux anomaly in 2014 compared to ten-year average (2005–14). Positive values are increased effluxes (or decreased influxes) and negative values are increased influxes (or decreased effluxes).

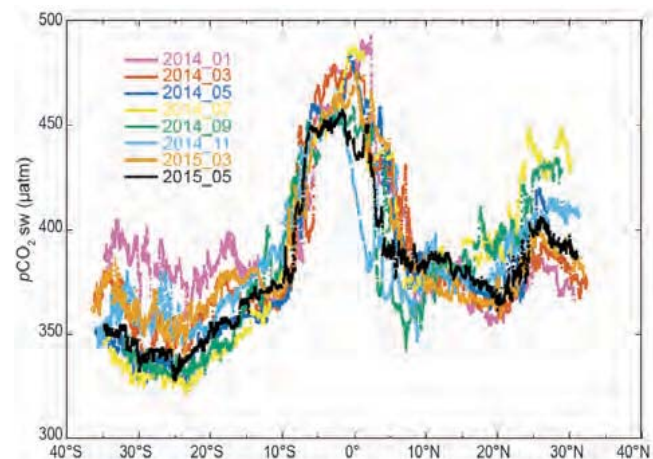


FIG. 3.29. CO₂ measurement from a ship of opportunity (SOOP) from New Zealand to Long Beach, CA, showing anomalously high surface water partial pressure of CO₂ ($p\text{CO}_2$) values in 2014 and 2015 in the anomalously warm surface water offshore of the California coast. Equatorial $p\text{CO}_2$ values are depressed in the boreal spring of 2014 and 2015 compared to climatological values.

Years	Mean C_{anth} Uptake (Pg C yr ⁻¹)	Reference
1960–69	1.1 ± 0.5	Le Quéré et al. 2015
1970–79	1.5 ± 0.5	Le Quéré et al. 2015
1980–89	2.0 ± 0.5	Le Quéré et al. 2015
1990–99	2.2 ± 0.5	Le Quéré et al. 2015
1994–2006	2.6 ± 0.5	Sabine and Tanhua 2010
2000–09	2.3 ± 0.5	Le Quéré et al. 2015
1994–2010	2.3 ± 0.5	Khatiwala et al. 2013
2000–10	2.9 ± 0.4	Kouketsu and Murata 2014
2005–14	2.6 ± 0.5	Le Quéré et al. 2015
2014	2.9 ± 0.5	Le Quéré et al. 2015

ing led to larger effluxes in the northwest Atlantic. A large negative anomaly in the northwest Pacific, perhaps related to a shift in the PDO, contributed to the higher-than-average 2014 ocean CO₂ uptake.

A recent synthesis of $p\text{CO}_2$ data in the western Arctic showed that the Arctic biogeochemical seascape is in rapid transition. An analysis of nearly 600 000 surface seawater $p\text{CO}_2$ measurements from 2003 to 2014 found $0.0109 \pm 0.0057 \text{ Pg C yr}^{-1}$ entered the ocean in the western Arctic coastal ocean (north of the Bering Strait) during this period, and that this uptake would be expected to increase by 30% under decreased sea ice cover conditions expected with Arctic warming (Evans et al. 2015). Reductions in ice cover may have a more moderate impact on other areas of the western Arctic, such as south of Bering Strait (Cross et al. 2014).

2) CARBON INVENTORIES FROM THE GO-SHIP SURVEYS

The CLIVAR/CO₂ Repeat Hydrography Global Ocean Ship-Based Hydrographic Investigations Program (GO-SHIP; www.go-ship.org/) collects high-quality surface-to-bottom water property measurements along transoceanic sections at decadal intervals. These data are essential for estimating decadal C_{anth} storage changes within the ocean interior. The extended multiple linear regression

method (eMLR) distinguishes these changes from large natural decadal changes in dissolved inorganic carbon (DIC) concentrations between cruises (e.g., Friis et al. 2005; Sabine et al. 2008). The method has recently been modified to permit basinwide estimates of C_{anth} trends by utilizing data from repeat hydrography cruises and climatological data from World Ocean Atlas 2013 (Sabine and Tanhua 2010; Locarnini et al. 2013; Zweng et al. 2013; Williams et al. 2015). Global-scale results from this modified eMLR approach indicate a C_{anth} uptake rate of $\sim 2.6 \text{ Pg C yr}^{-1}$ (1994–2006). This estimate is consistent (within uncertainties) with model-based (Khatiwala et al. 2013; Talley et al. 2016) and data-based estimates (Table 3.1) for this period.

C_{anth} storage rates vary widely regionally (Fig. 3.30), ranging from 0.1 ± 0.02 to $2.2 \pm 0.7 \text{ mol C m}^{-2} \text{ yr}^{-1}$ (Williams et al. 2015). For comparison, the 2.3–2.9 Pg C yr⁻¹ global mean uptake rate estimates above correspond to a global mean C_{anth} storage rate between 0.53 and 0.67 mol C m⁻² yr⁻¹. Updating regional storage estimates with measurements from the most recent GO-SHIP hydrographic surveys is an ongoing effort. Recent estimates (Fig. 3.30b) suggest greater storage in the Atlantic in the recent decade than in the preceding decade (Woosley et al. 2016), but consistent storage between the two decades in the Pacific.

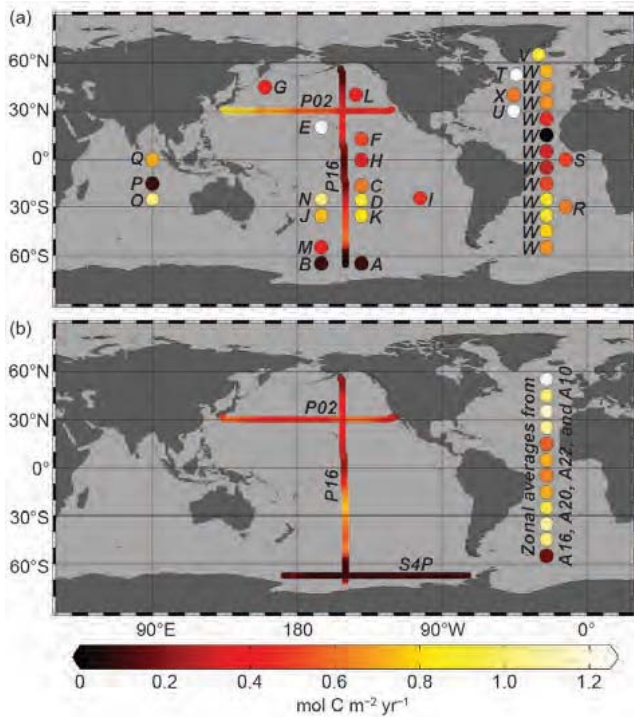


FIG. 3.30. Regional C_{anth} (anthropogenic carbon) storage rate estimates in literature as colored dots with positions corresponding to the approximate centers of the broad regions considered. Estimates are from: A. Williams et al. (2015), B. Sabine et al. (2008), C. Sabine et al. (2008), D. Peng et al. (2003), E. Peng et al. (2003), F. Murata et al. (2009), G. Wakita et al. (2010), H. Sabine et al. (2008), I. Waters et al. (2011), J. Waters et al. (2011), K. Waters et al. (2011), L. Sabine et al. (2008), M. Matear and McNeil (2003), N. Murata et al. (2007), O. Murata et al. (2010), P. Peng et al. (1998), Q. Peng et al. (1998), R. Murata et al. (2008), S. Peng and Wanninkhof (2010), T. Friis et al. (2005), U. Tanhua et al. (2007), V. Olsen et al. (2006), W. Wanninkhof et al. (2010), and X. Quay et al. (2007). Storage rate estimates that use data from cruises in the year 2011 or afterward are mapped in (b), and all other estimates are mapped in (a). Atlantic estimates in (b) are from Woosley et al. (2016). Colored lines are provided representing preliminary storage rate estimates along the labeled P16 and P02 sections in the decades spanning the (a) 1990s to 2000s and (b) 2000s to 2010s occupations. The similar line in (b) for S4P is from Williams et al. (2015).